Eur. Phys. J. B (2012) 85: 324
DOI: 10.1140/epjb/e2012-30267-y

THE EUROPEAN PHYSICAL JOURNAL B

Regular Article

Plasmon satellites in valence-band photoemission spectroscopy

Ab initio study of the photon-energy dependence in semiconductors

M. Guzzo[1,a,b], J.J. Kas[2], F. Sottile[1,b], M.G. Silly[3], F. Sirotti[3], J.J. Rehr[2], and L. Reining[1,b]

[1] Laboratoire des Solides Irradiés, École Polytechnique, CNRS, CEA-DSM, 91128 Palaiseau, France
[2] Department of Physics, University of Washington, Seattle, 98195 WA, USA
[3] Synchrotron-SOLEIL, BP 48, Saint-Aubin, 91192 Gif sur Yvette Cedex, France

Received 27 March 2012 / Received in final form 15 June 2012
Published online 24 September 2012 –

Abstract. We present experimental data and theoretical results for valence-band satellites in semiconductors, using the prototypical example of bulk silicon. In a previous publication we introduced a new approach that allows us to describe satellites in valence photoemission spectroscopy, in good agreement with experiment. Here we give more details; we show how the the spectra change with photon energy, and how the theory explains this behaviour. We also describe how we include several effects which are important to obtain a correct comparison between theory and experiment, such as secondary electrons and photon cross sections. In particular the inclusion of extrinsic losses and their dependence on the photon energy are key to the description of the energy dependence of spectra.

1 Introduction

Photoemission spectroscopy (PES) is an established tool for the analysis of the electronic structure of solids and molecules. Its increasing capability in energy-resolution and flexibility has made more urgent the need for advanced theoretical approaches able to cope with the huge range of systems being measured and with the high precision needed to match the experiment [1]. One powerful and commonly used framework is based on the one-particle Green's function $G(\mathbf{x}, \mathbf{x}', t, t')$ [2], which describes the propagation of one particle in the system. A popular approximation for the propagator is the GW approximation [3], which has proven to be successful in a variety of systems calculations of photoemission band gaps [4,5]. The quantity to be compared with experiment is the one-particle spectral function $A(\omega)$ which is proportional to the imaginary part of G. The main features of the spectral function $A(\omega)$ are quasiparticle (QP) peaks with finite lifetime. In addition, the spectral function shows incoherent satellite structures. In *sp* semiconductors these satellites are mainly due to the excitation of plasmons (both surface and bulk). Satellites in photoemission spectroscopy have been extensively studied for core-level spectra [6–8], while for valence-band spectroscopy there has been much less effort [9–11]. Still, valence-band satellites have been measured in a number of systems and are at the center of the debate around some highly interesting systems like transition metal oxides. In a previous work [12] we introduced a new method to describe satellites with an improved description of the intrinsic spectral function, including effects beyond the latter. In particular our method includes the dependence of the spectrum on photon energy. In this paper we present details of the method. We also show how the photoemission spectrum of silicon depends on the photon energy and we give a prediction for the trend at very high photon energies.

1.1 The sudden approximation and the three-step model

When making comparisons between theory and experiment, it is worth noting that there is not a complete coincidence between the spectral function $A(\omega)$ and the PES spectrum. This is because $A(\omega)$ only describes the propagation of the hole created by the incoming photon, while completely neglecting the losses of the photoelectron before it leaves the system. The use of $A(\omega)$, within these limits, to describe PES is known as the *sudden approximation*. While this approximation simplifies the description of PES, it is safe to say that it is never actually true. In fact it turns out that the losses of the outgoing photoelectrons are roughly the same at all photon energies. This is the result of two competing processes [6]:

(i) the reduction of the inelastic scattering cross section of electrons as their kinetic energy increases. As the photon energy increases, the average kinetic energy

[a] e-mail: matteo.guzzo@polytechnique.edu
[b] European Theoretical Spectroscopy Facility (ETSF), http://www.etsf.eu

of the electrons in the solid will increase. With it, the average loss probability per electron will decrease;

(ii) the increase of the mean free path of electrons as their kinetic energy increases. A larger mean free path will correspond to a greater maximum depth of a hole for which the corresponding photoelectron is fast enough to reach the surface and be detected. This implies that, on average, electrons will have to travel through a thicker layer of atoms before escaping the material. This way, the energy-loss probability will increase.

These two phenomena make the losses of the photoelectrons non-negligible at any photon energy. The good news is that the effect of these losses on the QP part of the spectrum is often only an overall renormalization of the peaks, which explains the success of the sudden approximation for the description of QP band structures. However, an appropriate calculation and interpretation of satellite structures in photoemission spectra requires one to go beyond the sudden approximation. A more complete, yet simplistic way of modeling the photoemission process is to divide it in three independent sequential steps:

1. optical excitation of the electron in the bulk;
2. travel of the excited electron to the surface;
3. escape of the photoelectron into vacuum.

This is known as the *three-step* model, as first proposed by Berglund and Spicer [13]. The total photoemission intensity is then given by the product of the probabilities of the three different processes. The first step is described by the one-particle spectral function $A(\omega)$. Losses coming from $A(\omega)$ are called *intrinsic* [6]. Step two is described by the electron energy-loss spectrum of the system and, along with step three, is considered part of the *extrinsic* losses. At this point, to get the total intensity, it would be sufficient to convolute $A(\omega)$ with the energy-loss spectrum. This case is referred to as the *sudden limit* [6]. However, this condition is met only at very high photon energies that are rarely accessed in usual PES conditions. In fact, there is quantum-mechanical interference between intrinsic and extrinsic losses, which is due to the interaction between the outgoing photoelectron and the hole it has left behind. The changes occurring in the photoemission spectrum following this kind of process, are referred to as *interference effects*. To describe this kind of processes one should in principle make use of a two-particle propagator [14], but it is possible to treat this effect in an approximate way retaining at the same time a good deal of physical insight. Within this picture, we use an optimized three-step model that attempts to overcome the shortcomings of its original formulation.

2 Theoretical framework

Our method is based on the exact equation of motion of the fully-interacting 1-particle electronic Green's function $G_\sigma(\mathbf{x},\mathbf{x}',t,t')$. The equation reads [15]

$$G = G_0 + G_0 V_H G + G_0 \varphi G + i G_0 v_c \frac{\delta G}{\delta \varphi}, \qquad (1)$$

where G_0 is the non-interacting Green's function, φ is a fictitious external perturbation that is set to zero at the end of the derivation, v_c is the bare Coulomb interaction, and all quantities are understood to be matrices in space, spin, and time. The Hartree potential V_H gives rise to screening to all orders. Spin only gives rise to a factor of 2, since we are interested here in non-magnetic systems where G is spin-diagonal.

2.1 Decoupling approximation for the Green's function

Linearizing V_H with respect to φ and assuming G and G^H diagonal on the same discrete basis yields a scalar equation for each matrix element $\mathcal{G} = G_{ii}$ which corresponds to a single state of the system [12,16]:

$$\mathcal{G}(t_1t_2) = \mathcal{G}^0_H(t_1t_2) + \mathcal{G}^0_H(t_1t_3)\bar{\varphi}(t_3)\mathcal{G}(t_3t_2) + i\mathcal{G}^0_H(t_1t_3)\mathcal{W}(t_3t_4)\frac{\delta\mathcal{G}(t_3t_2)}{\delta\bar{\varphi}(t_4)}, \qquad (2)$$

where $\mathcal{G}^0_H$ is the Hartree Green's function in the limit of vanishing external potential; $\bar{\varphi} = \varepsilon^{-1}\varphi$ is the screened external perturbation potential;

$$\mathcal{W}(t_3t_4) = \int dr dr' |\phi(r)|^2 |\phi(r')|^2 W(rr't_3t_4) \qquad (3)$$

is a diagonal matrix element of the screened Coulomb interaction W; ϕ is the single-particle wavefunction of the corresponding state; and ε^{-1} is the inverse microscopic dielectric function. It is worth noting that in equation (2) the approximation $\delta G/\delta\bar{\varphi} = GG$ – which corresponds to the Random-Phase Approximation (RPA) for the response to the screened external potential $\bar{\varphi}$ – gives back the GW approximation [3], which is hence included in the current approximation. The solution of equation (2) at vanishing φ, for a single occupied state, is

$$\mathcal{G}(t_1t_2) = \mathcal{G}^0_H(t_1t_2)\exp\left[-i\int_{t_1}^{t_2} dt' \int_{t'}^{t_2} dt'' \mathcal{W}(t't'')\right]. \qquad (4)$$

We assume that $\mathcal{W}$ can be represented by a sum of N_p poles $\tilde{\omega}_j$ with strength λ_j, which is exact for infinite N_p:

$$\mathcal{W}(\tau) = \sum_j^{N_p} \lambda_j \left[e^{i\tilde{\omega}_j\tau}\theta(-\tau) + e^{-i\tilde{\omega}_j\tau}\theta(\tau)\right], \qquad (5)$$

where $\tau = t - t'$. Using equation (5), the double integration of $\mathcal{W}$ in equation (4) is then analytically feasible. Once this is carried out, the matrix elements of the Green's function read

$$\mathcal{G}(\tau) = i\theta(-\tau)e^{-i(\epsilon+i\Gamma)\tau}\exp\left[\sum_j^{N_p} a_j(1 - e^{i\tilde{\omega}_j\tau})\right], \qquad (6)$$

with $a_j = \lambda_j/\tilde{\omega}_j^2$. In equation (6), the first exponent $\epsilon + i\Gamma$ is the *complex* QP energy within the GW approximation. The GW correction to the Hartree energy naturally

emerges from the integral of $\mathcal{W}$ in equation (4), provided that the same level of approximation is used for $\mathcal{W}$ in the GW self energy. The second exponential term provides for renormalization and formation of satellites at all orders. After having expanded and Fourier-transformed the latter, $A(\omega) = 1/\pi|\,\mathrm{Im}\mathcal{G}(\omega)|$ becomes

$$A(\omega) = \frac{\Gamma}{\pi} e^{-\sum_j^{N_p} a_j} \left[\frac{1}{(\omega-\epsilon)^2+\Gamma^2} + \sum_j^{N_p} \frac{a_j}{(\omega-\epsilon+\tilde{\omega}_j)^2+\Gamma^2} + \frac{1}{2}\sum_{jk}^{N_p} \frac{a_j a_k}{(\omega-\epsilon+\tilde{\omega}_j+\tilde{\omega}_k)^2+\Gamma^2} + \frac{1}{6}\sum_{jkl}^{N_p} \frac{a_j a_k a_l}{(\omega-\epsilon+\tilde{\omega}_j+\tilde{\omega}_k+\tilde{\omega}_l)^2+\Gamma^2} + \ldots \right]. \quad (7)$$

Equation (7) shows how the spectral function can be expanded as a sum of poles, which are regrouped here in different terms following the corresponding order. The zeroth order (first term) is the QP peak, centered at the QP energy ϵ. The following terms are centered at $\omega - n\tilde{\omega}_j$ (at order n, giving rise to the n-th satellite replica for that frequency) with a weight decreasing exponentially with n. In general, the weights a_j are of the order of $0.1/N_p$.

The electron energy-loss function of bulk silicon has a well-defined single-peaked shape, centered at 16.7 eV. This fact justifies the use of a single plasmon-pole model which is equivalent, in the above formulation, to the case $N_p = 1$.

2.2 Calculation of extrinsic losses and interference effects

In order to take the extrinsic and interference terms into account, we use the theoretical formalism of Hedin, Michiels, and Inglefield [6], which includes all three effects, i.e., intrinsic, extrinsic, and interference. In addition, the theory is based on a semi-infinite model of the system, and thus the satellite spectrum depends on the average distance traveled by the photo-electron through the surface. However, these calculations use a rather crude approximation for the valence electrons, treating them as localized states. The strategy is thus to use this complete model to calculate the extrinsic and interference terms only, replacing the intrinsic contribution with the more rigorous calculations detailed in the previous section. One might worry that the intrinsic spectrum would then not include effects due to the semi-infinite model. However, we find that the intrinsic spectrum is quite insensitive to distance from the surface. The theory accounts for the satellites in the PES spectrum in terms of a spectral function $A(\omega)$ of exponential form consistent with equation (7), which allows us to combine the two approaches. In this approach the photocurrent is given by

$$\langle J_k(\omega)\rangle = \sum_i |M_{ik_0}|^2 \int_0^\infty e^{-a} \int_{-\infty}^\infty e^{i(\omega_0-\epsilon_k+\epsilon_i)t} \quad (8)$$

$$\times \exp\left[\int \gamma_{ik}(\omega)(e^{-i\omega t}-1)\, d\omega\right] dt\, dz_c, \quad (9)$$

where

$$a \approx \int d\omega\, \gamma_{ik}(\omega) = 2z_c \mathrm{Im}\tilde{k} + a^i_{int}. \quad (10)$$

Here ω_0 is the photon-frequency, $k_0 = \sqrt{2(\omega_0+\epsilon_i)}$ is the photo-electron momentum at threshold, and we have made the approximation that the matrix elements $M_{ik} = \langle i|d|k\rangle$ are roughly constant over the range of photo-electron energies of interest, i.e., from a few multiples of the plasmon energy below the photon energy to threshold where $\epsilon_k = \omega$. The function $\gamma_{ik}(\omega)$ characterizes the losses due to the excitation of single plasmons of energy $\omega_{\mathbf{q}}$ and can be split into intrinsic, extrinsic and interference contributions,

$$\gamma_{ik}(\omega) = \sum_{\mathbf{q}} |g_{\mathbf{q}}|^2 \delta(\omega-\omega_q) = \gamma_i^{int} + \gamma_k^{ext} + \gamma_{ik}^{inf}. \quad (11)$$

We calculate the extrinsic and interference terms by assuming that the intrinsic amplitude is independent of the initial (valence) state, which gives the amplitudes,

$$|g_{\mathbf{q}}| = \left| \frac{V^{\mathbf{q}}(z_c)}{\omega} + \frac{i}{\kappa}\int_{-\infty}^{z_c} e^{i(\tilde{k}-\kappa)(z-z_c)} V^{\mathbf{q}}(z) dz \right| \quad (12)$$

where the solid occupies the space $z > 0$. The first term gives the intrinsic amplitude, while the second term gives the extrinsic, and the cross terms give the interference, i.e.,

$$|g_q|^2 = |g_q^{\mathrm{int}}|^2 + |g_q^{\mathrm{ext}}|^2 + 2\mathrm{Re}[g_q^{\mathrm{int}} g_q^{\mathrm{ext}}]. \quad (13)$$

The complex wave numbers κ and $\tilde{k}$ are given by

$$\kappa = \sqrt{2(\omega_0+\phi+\epsilon_F+i\Gamma(\omega+\epsilon_k)) - |\mathbf{Q}+\mathbf{K}|^2}, \quad (14)$$

$$\tilde{k} = \sqrt{k^2 + 2(\phi+\epsilon_F+i\Gamma(\epsilon_k)}, \quad (15)$$

and correspond to a time-inverted LEED state,

$$|\tilde{k}\rangle = e^{i\mathbf{K}\cdot\mathbf{R}}\left[\theta(z)e^{-i\tilde{k}^* z} + \theta(-z)e^{-ikz}\right]. \quad (16)$$

Here ϵ_F is the Fermi energy and ϕ is the work function. Further, bold capitals denote components of the vector perpendicular to the z direction (parallel to the surface). With the above definitions, $\epsilon_k = k^2$, and ω is measured relative to the valence binding energy so that the first detectable photo-electron comes at $\omega = \epsilon_k = 0$.

In order to evaluate the relative weights of various contributions to the PES signal, we use the Inglesfield fluctuation potential inside the solid (contributions outside being negligible) [6]. We then calculate the weight of the extrinsic and interference $a^{extinf}(\omega_0) = a^{ext}(\omega_0) + a^{inf}(\omega_0)$

Table 1. Values of the correction term a^{extinf} including extrinsic losses and interference effects and relative width (inverse lifetime) η for a set of photon energies ω_0.

ω_0 (eV)	a^{extinf}	η
200	0.432	2.882
480	0.479	1.085
800	0.530	0.570
1200	0.568	0.341
2000	0.609	0.178
5000	0.669	0.066
10000	0.703	0.027

contributions to the PES due to plasmons of energy $\omega_p = 16.7$ eV, at a given photon energy ω_0, i.e.,

$$a^{\text{extinf}}(\omega_0) = \int dk \gamma_k^{\text{ext}}(\omega_0) + \gamma_k^{\text{inf}}(\omega_0). \quad (17)$$

We incorporate these contributions in our total spectral function correcting the intrinsic contribution of Section 2.1 with the addition of $a^{extinf}(\omega_0)$ i.e.,

$$\bar{a}_i = a_i^{int} + a^{extinf}(\omega_0), \quad (18)$$

where i denotes the valence state, a_i^{int} is the intrinsic weight of the pole as it appears in equation (7) for the case $N_p = 1$. We can also calculate the width of the extrinsic + interference satellites and account for this by replacing the widths Γ in equation (7), i.e.

$$\Gamma \rightarrow \Gamma + n\,\eta(\omega_0), \quad (19)$$

η being the width (related to the dispersion of the plasmon) of the extrinsic plasmon peak at a given photon energy ω_0 and n the number of plasmon excitations involved, i.e. the order of the expansion in equation (7). Values of ω_0, a^{extinf} and η are listed in Table 1.

2.3 Additional effects

2.3.1 Lifetime of intrinsic plasmons

We must include a correction for the finite lifetime of intrinsic plasmons, which is infinite in (7) because of the plasmon-pole model we are using for the intrinsic part. Therefore, an additional width of 1.5 eV [17] is added to the inverse lifetime of extrinsic plasmons η.

2.3.2 Photon cross sections

Photon cross sections are taken from references [18,19]. For each element, the tables give the relative photon cross section of the atomic orbitals, calculated within the Hartree-Fock approximation. We have to use the atomic data for bulk silicon; since we are in a solid, the atomic character is mixed. The four valence bands of silicon contain two s electrons and two p electrons. The character of each band is calculated by projecting the wavefunctions

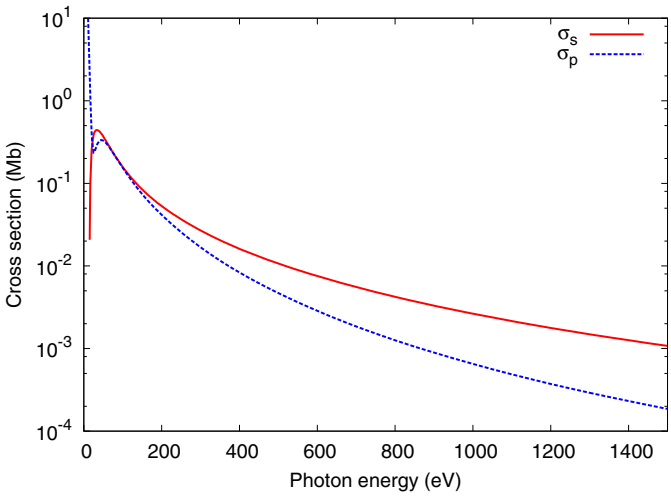

Fig. 1. (Color online) Photon cross sections, from reference [18]. Red solid line shows the values for the $3s$ electrons, while the blue dashed line shows the $3p$ electrons cross sections.

onto spherical harmonics inside a sphere centered on the Si ion. The s and p character of each band sum up to one. We have then the following values:

Band	#1	#2	#3	#4
s-type	0.95	0.75	0.25	0.05
p-type	0.05	0.25	0.75	0.95

In this picture, the relative weight of a photoemission peak will be the consequence of the s_k and/or p_k character of the corresponding state k. To include this effect in the spectral function, we can define an effective $\tilde{A}$ so that

$$\tilde{A}(\omega) = \sum_k (s_k\sigma_s + p_k\sigma_p)A_k(\omega), \quad (20)$$

where A_k is the (intrinsic or corrected) spectral function of a single state k and σ_s and σ_p are the photon cross sections for s and p electrons, tabulated in references [18,19] and shown in Figure 1 up to 1500 eV. The inclusion of cross-section effects is very important to reproduce the relative weight of s and p peaks in the photoemission spectrum (which can differ by an order of magnitude) and the respective changes at different photon energies.

2.3.3 Secondary electrons

The background of secondary electrons is calculated using the effective intrinsic spectral function $\tilde{A}(\omega)$, assuming that each peak in the intrinsic spectrum produces a constant flux of secondary electrons (i.e. a step function) at all binding energies greater than the quasiparticle energy ϵ. This is commonly known as a *Shirley* background [20]. The calculation of the background is achieved by the following integration of $\tilde{A}(\omega)$:

$$\mathcal{B}(\omega) = \int_\omega^\mu d\omega' \tilde{A}(\omega'), \quad (21)$$

where $\mathcal{B}$ is the background of secondary electrons. The final quantity that has to be compared with experimental data is given by the photocurrent $J(\omega)$ defined as:

$$J(\omega) = \alpha\tilde{A}(\omega) + \beta\mathcal{B}(\omega), \tag{22}$$

where α and β are two parameters that must be fixed to match the signal/background ratio in the experimental data. β is to be determined using the high binding-energy limit (where $\tilde{A}(\omega) \sim 0$) and then we fix α so as to match the QP peak intensity. The calculated background could also be subtracted from the experimental curves, in case one wishes e.g. to evaluate the intensity of satellites (see below).

3 Experimental setup

Valence PES measurements were performed at the UHV photoemission experimental station of the TEMPO beamline [21] at the SOLEIL synchrotron radiation source. Linearly polarized photons from the Apple II type Insertion Device (HU44) were selected in energy using a high resolution plane grating monochromator with a resolving power $E/\Delta E = 5000$. The end-station chamber (base pressure 10^{-10} mbar) is equipped with a modified SCIENTA-200 electron analyzer with a delay-line 2D detector which optimizes the detection linearity and signal/background ratio [22]. The overall energy resolution was better than 200 meV. The photon beam impinges on the sample at an angle of 43°, and photoelectrons were detected around the sample surface normal with an angular acceptance of ±6°. A doped n^+-type Si(001) wafer ($N_D \simeq 2 \times 10^{-18} P$ atoms/cm^3) was cleaned from the native oxide by flash annealing at 1100 °C after prolonged degassing at 600 °C in ultra-high vacuum. The silicon surface annealed at 300 °C to prevent surface etching was then hydrogenated in a partial pressure of activated hydrogen about 2×10^{-8} mbar for 20 min. At 800 eV kinetic energy the Si Brillouin zone (BZ) is observed with an emission angle slightly smaller than 5°. The Fermi level was obtained by measuring a clean Au(111) surface. The measured photoemission map at 800 eV was integrated over the spectral intensity originated by two BZ. For lower photon energies it was not possible to have a complete integration of the BZ. Considering the ratio between satellites and QP peaks – which is a key quantity for our analysis – independent of the integration on the BZ (as our theory assumes), justifies the use of photon energies lower than 800 eV for comparison with theory.

4 Results

We have measured PES data for several photon energies between 200 and 800 eV. Using our procedure we have calculated the photoemission spectra for a range of photon energies between 200 eV and 10 keV. A standard *GW* calculation was performed using the ABINIT code [23]. The *GW* calculation was used to evaluate the parameters of equation (7), under the assumption that $\mathrm{Im}W \sim 1/\pi\,\mathrm{Im}\Sigma$ [24], hence using an RPA screening. We calculated the correction paramenters for extrinsic losses and interference effects as described earlier in Section 2.2, and eventually included cross-section effects as in equation (20). The graph in Figure 2 shows the calculated photoemission spectra $\tilde{A}(\omega)$ for a number of selected photon energies, from 200 eV to 10 keV. In this figure the intensity of the curves has been scaled so that the spectra match in the QP region. Varying the photon energy, there is a small change in the QP part of the spectrum – between −15 and 0 eV from the Fermi energy – due to cross-section effects[1]. The most apparent change is in the satellite part, i.e. below −15 eV, where three satellites are visible. Our calculations show that with increasing photon energy the satellites have a tendency to show more structures. More importantly, the relative weight of satellites increases as the photon energy increases. This trend is the same as the one found in the experimental data, as reported in Figure 3. In this figure we also include data from reference [25]. We assume a complete integration of the BZ. The ratio between the weight of the first satellite – taken between −33 and −15 eV – and the QP peaks has been calculated, both in the theoretical and experimental case, evaluating the integral under the curves. The calculated background has been removed from the experimental curves before the evaluation of the integrals. The set of experimental values is small with respect to what would be needed to perform an exhaustive comparison with theory. For smaller photon energies (between 200 and 400 eV), the ratios are systematically overestimated. Partial integration of the BZ, caused by the low photon energy used, is probably the cause of the overestimation

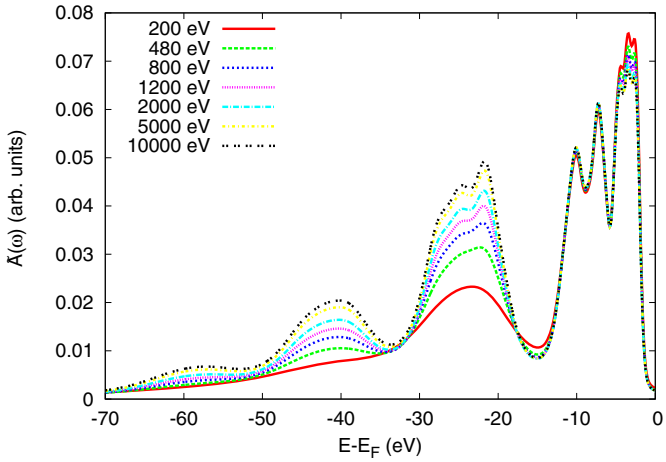

Fig. 2. (Color online) Calculated spectrum $\tilde{A}(\omega)$ for several photon energies between 200 eV and 10 keV. The spectra include the effect of cross sections and extrinsic losses. The curve intensities are aligned to match in the QP region, between −15 and 0 eV, to highlight the relative change of the satellite spectral weight, i.e. below −15 eV. The Fermi energy is at 0 eV.

[1] Additional variations related to different integrations of the BZ (found in experiment) are here neglected.

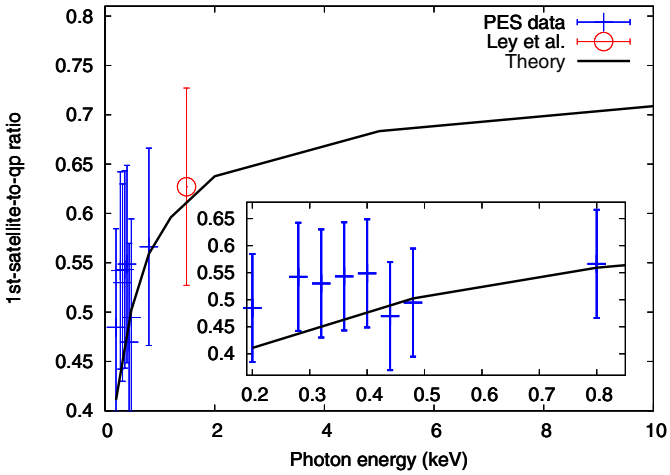

Fig. 3. (Color online) Intensity ratio between the first satellite and the QP part of the spectrum as a function of the photon energy. Our experimental data (blue crosses) are compared to theoretical calculation (black solid line). An additional point (red circle) taken from [25] has also been included for comparison. The inset shows a detail of the same plot.

of the satellite/QP ratio in these cases. In fact, the lower the photon energy, the smaller the portion of BZ measured for the same emission angle [1]. In our theory, we assume that QP states do not mix and each QP state has its own plasmons. This is a good approximation if done to evaluate a total spectrum, which is the result of a sum over all the states, i.e. over the whole BZ. Moreover our background is calculated assuming a uniform integral over the full BZ. Taken into account this and the inherent difficulty to precisely determine the points that define the QP region and the first satellite, our experimental points have an absolute error of ±0.1.

Theory allowed us to calculate spectra at high values of photon energies that we could not reach in experiment. Figure 3 shows how the satellite/QP ratio increases significantly from 0 up to 1−2 keV and how above 5−10 keV there is a sort of saturation effect. However, the satellite shape continues to sharpen (show more structure) as the photon energy increases. The origin of this sharpening is to be found in the width of extrinsic plasmon peak (see Tab. 1), which decreases as the photon energy increases and changes more than the intensity of plasmons, hence being the crucial quantity in the equation that determines most changes in the shape of satellites, as it appears from our analysis. The behavior of the satellite/QP ratio is more complicated due to the inelastic mean free path (IMFP) of the photoelectron, which increases with energy. This increase in IMFP gives rise to two competing effects: (i) the increased IMFP allows electrons from deeper in the material to escape, which increases the strenth of the extrinsic plasmon peak; (ii) the IMFP is (inversely) a measure of the probability of scattering plasmons, thus a larger IMFP means that the contribution to the plasmon peak from each hole is lowered.

5 Conclusion

In conclusion we have shown how to describe ab initio satellites in valence-band photoemission spectroscopy. Our method is able to describe multiple excitation of plasmons including lifetimes. This gives an accurate description of the intrinsic part of the spectrum. A number of effects that are not removable from experiment have to be added to the theoretical calculations to obtain an appropriate comparison with experimental data. The photon-energy dependence of satellites was studied including, in the spectral function $A(\omega)$, correcting terms for the intensity and width of extrinsic plasmon peaks, also taking into account interference effects. We compared the theoretical results with our experimental photoemission data, taken at several photon energies, between 200 and 800 eV. Using our theoretical approach, we could give a prediction on a larger range of energies. We evaluated the ratio between the weight of the first satellite and of the QP peaks. Satellites grow bigger with respect to QP peaks as the photon energy increases, until the sudden limit is reached, above 5−10 keV. The measured data are in agreement with the theoretical curve. The main physical process behind the increase of satellite weight appears to be the variation of the IMFP of photoelectrons. The evaluation of extrinsic and interference effects could be done in a relatively straightforward way thanks to the formulation we introduced for the Green's function and the spectral function. The same would not have been possible if one stayed within the *GW* approximation, where spurious plasmaron excitations spoil the satellite spectra [12] and multiple satellites are absent.

We acknowledge ANR (project #: NT09-610745) for funding, IDRIS and CCRT for computer time (GENCI-544 project). J.J. Rehr and J.J. Kas acknowledge the support of US Department of Energy, Basic Energy Sciences, Grant No. DE-FG03-97ER45623.

References

1. A. Damascelli, Z. Hussain, Z.-X. Shen, Rev. Mod. Phys. **75**, 473 (2003)
2. A.L. Fetter, J.D. Walecka, *Quantum theory of Many-Particle Systems* (MacGraw-Hill, New York, 1971)
3. L. Hedin, Phys. Rev. **139**, A796 (1965)
4. W. Aulbur, L. Jonsson, J. Wilkins, Solid State Phys. **54**, 1 (2000)
5. F. Aryasetiawan, O. Gunnarsson, Rep. Prog. Phys. **61**, 237 (1998)
6. L. Hedin, J. Michiels, J. Inglesfield, Phys. Rev. B **58**, 15565 (1998)
7. F. Bechstedt, *Principles of Surface Physics* (Springer, 2003), Chap. 5, pp. 199–201
8. F. Offi et al., Phys. Rev. B **76**, 085422 (2007)
9. L. Hedin, J. Phys.: Condens. Matter **11**, R489 (1999)
10. C.-O. Almbladh, L. Hedin, *Handbook on Synchrotron Radiation* (North-Holland, Amsterdam, 1983), Chap. 8
11. A.S. Kheifets et al., Phys. Rev. B **68**, 233205 (2003)

12. M. Guzzo, G. Lani, F. Sottile, P. Romaniello, M. Gatti, J.J. Kas, J.J. Rehr, M.G. Silly, F. Sirotti, L. Reining, Phys. Rev. Lett. **107**, 166401 (2011)
13. C.N. Berglund, W.E. Spicer, Phys. Rev. **136**, A1030 (1964)
14. F. Bechstedt, K. Tenelsen, B. Adolph, R. DelSole, Phys. Rev. Lett. **78**, 1528 (1997)
15. L.P. Kadanoff, G. Baym, *Quantum Statistical Mechanics* (W.A. Benjamin Inc., New York 1964)
16. G. Lani, P. Romaniello, L. Reining, New J. Phys. **14**, 013056 (2012)
17. B. Arnaud, S. Lebègue, M. Alouani, Phys. Rev. B **71**, 035308 (2005)
18. J. Yeh, I. Lindau, At. Data Nucl. Data Tables **32**, 1 (1985)
19. J.H. Scofield, *Theoretical photoionization cross sections from 1 to 1500 kev*, Tech. Rep. UCRL-51326, Lawrence Livermore National Laboratory, 1973
20. D.A. Shirley, Phys. Rev. B **5**, 4709 (1972)
21. F. Polack et al., AIP Conf. Proc. **1234**, 185 (2011)
22. N. Bergeard et al., J. Synch. Rad. **18**, 245 (2011)
23. X. Gonze, G.-M. Rignanese, M. Verstraete, J.-M. Beuken, Y. Pouillon, R. Caracas, F. Jollet, M. Torrent, G. Zerah, M. Mikami, P. Ghosez, M. Veithen, J.-Y. Raty, V. Olevano, F. Bruneval, L. Reining, R. Godby, G. Onida, D. Hamann, D. Allan, Z. Kristallogr. **220**, 558 (2005)
24. F. Aryasetiawan, L. Hedin, K. Karlsson, Phys. Rev. Lett. **77**, 2268 (1996)
25. L. Ley, S. Kowalczyk, R. Pollak, D.A. Shirley, Phys. Rev. Lett. **29**, 1088 (1972)